2008 IEEE International Conference on
Robotics and Automation
Pasadena, CA, USA, May 19-23, 2008

Control of Swarms Based on Hydrodynamic Models

Luciano C. A. Pimenta, Nathan Michael, Renato C. Mesquita, Guilherme A. S. Pereira, Vijay Kumar

Abstract— **We address the problem of pattern generation in obstacle-filled environments by a swarm of mobile robots. Decentralized controllers are devised by using the Smoothed Particle Hydrodynamics (SPH) method. The swarm is modelled as an incompressible fluid subjected to external forces. Actual robot issues such as finite size and nonholonomic constraints are also addressed. Collision avoidance guarantees are discussed. Finally, in the absence of obstacles, we prove for the first time stability and convergence of controllers based on the SPH.**

I. INTRODUCTION

The focus of this work is on using analogies with fluid dynamics models to control swarms of robots. The main motivation stems from the fact that a great variety of characteristics desirable for a large group of robots may be observed in fluids. Some examples of such characteristics are: (i) fluids are easily deformed, (ii) fluids can easily flow around objects, and (iii) the flow field variables and also the fluid phase can be easily manipulated in order to design desired behaviors.

Other works have already mimicked fluid behaviors to control large groups of robots. The authors of [1] used *Stokesian Dynamics*. By using this technique the robots had the behavior of particles suspended in a fluid and the group shape could be controlled without losing the group coherence. In [2] the kinetic theory of gases was used to sweep a group of robots through a bounded region.

In this work we are interested in the so-called *pattern generation problem*, which may be stated as follows:

Given N robots and any initial spatial distribution, the geometry of the environment with static obstacles defining a compact domain $\Omega \subset \mathbb{R}^2$, and a curve $\Gamma : I \to \Omega$, where $I \subset \mathbb{R}$, find a controller which enables the robots, without colliding with static obstacles and each other, to form Γ.

Possible applications of an efficient solution to this task are surveillance and cordoning off of hazardous areas. We are interested in a decentralized solution which scales from tens to hundreds of robots. Some approaches as in [3] assume that each robot knows the positions of all the others. To achieve scalability, it is more interesting to have an approach that relies only on local information. Approaches that depend on labelling the robots are also hard to scale since it may be difficult to uniquely identify agents in the swarm. Approaches based on leader-follower controllers are examples of this class [4], [5]. Behavior-based techniques for formation control are applied in [6] and [7] but in these cases proofs of stability of the given formation are not discussed.

The use of artificial potential fields to address the pattern generation task in the absence of obstacles is discussed in [8] and [9]. In these works, scalable approaches are derived and proofs of convergence and stability are given. The problem of staying connected during the task is also considered in [9].

In contrast to the others, in this work we use the *Smoothed Particle Hydrodynamics* method to model the swarm emulating an incompressible fluid in an obstacle-filled environment. We deal with static obstacles by computing a global potential function and using virtual particles. The incompressible fluid model allows for a loose way of controlling the connectivity of the swarm. We provide a decentralized and scalable approach which relies only on local information. Moreover, there is no need to label the agents in the swarm.

II. SMOOTHED PARTICLE HYDRODYNAMICS

The Smoothed Particle Hydrodynamics (SPH) is a *mesh-free particle* numerical method. It is a particle numerical method since it employs a set of finite number of disordered discrete particles to represent the state of the simulated system. It is mesh-free due to the fact that it is not necessary to generate a mesh to provide connectivity of the particles. Additionally, SPH is considered a *Lagrangian* method, which means that the individual particles are modelled in space and in time in contrast to Eulerian methods that model the flux of material through a control volume fixed in space.

The continuum governing equations of fluid dynamics capture three salient phenomena: (i) conservation of mass; (ii) conservation of momentum; and (iii) conservation of energy. For inviscid compressible fluids, in the absence of heat flux, the Lagrangian description is given by:

$$\frac{D\rho}{Dt} = -\rho \nabla \cdot \mathbf{v}\,, \tag{1}$$

$$\frac{D\mathbf{v}}{Dt} = -\frac{\nabla P}{\rho}\,, \tag{2}$$

$$\frac{De}{Dt} = -\left(\frac{P}{\rho}\right) \nabla \cdot \mathbf{v}\,, \tag{3}$$

where ρ is density, $\mathbf{v}$ is velocity, e is the internal energy per unit of mass, P is the hydrostatic pressure, ∇ is the gradient operator, $\nabla \cdot ()$ is the divergence, and D/Dt is the *total time derivative* which is physically the time rate of change following a moving fluid element.

In the SPH method, the continuum equations of fluid dynamics are converted to a set of ordinary differential equations, where each one controls the evolution of an attribute of a specific particle. This conversion is performed by

L. C. A. Pimenta, R. C. Mesquita, and G. A. S. Pereira are with the Department of Electrical Engineering, Universidade Federal de Minas Gerais, Belo Horizonte, MG, 31270-901, Brazil. {lucpim, renato, gpereira}@cpdee.ufmg.br

N. Michael and V. Kumar are with the GRASP Laboratory, University of Pennsylvania, Philadelphia, PA 19104, USA. {nmichael, kumar}@seas.upenn.edu

978-1-4244-1647-9/08/$25.00 ©2008 IEEE.

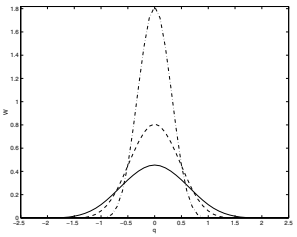

Fig. 1. One-dimensional kernel function. The solid, dashed, and dashdot lines correspond respectively to $h = 1$, $h = 0.75$, and $h = 0.5$.

using differentiable interpolation kernels, which approximate a delta function. The kernel is chosen to satisfy $\int_{\Upsilon} W(\mathbf{q} - \mathbf{q}', h)d\mathbf{q}' = 1$ and $\lim_{h\to 0} W(\mathbf{q} - \mathbf{q}', h) = \delta(\mathbf{q} - \mathbf{q}')$, where Υ is the volume that contains $\mathbf{q}$, h is a parameter that controls the influence area of W, and $\delta(\mathbf{x} - \mathbf{x}')$ is the Dirac delta function. The error in approximating the integral representation of a function by summations of the function evaluated at particle locations weighted by interpolation kernels is $O(h^2)$ [10]. In this work, we use the cubic spline:

$$W(\mathbf{q}, h) = \frac{10}{7\pi h^2} \begin{cases} 1 - \frac{3}{2}\kappa^2 + \frac{3}{4}\kappa^3 & \text{if} \quad 0 \le \kappa \le 1\,, \\ \frac{1}{4}(2-\kappa)^3 & \text{if} \quad 1 \le \kappa \le 2\,, \\ 0 & \text{otherwise}\,, \end{cases} \tag{4}$$

where $\kappa = \|\mathbf{q}\|/h$. It can be observed that the function support is determined by $2h$ (see Fig. 1).

The SPH conservation equations for a particle i are:

$$\rho_i = \sum_j m_j W(\mathbf{q}_{ij}, h)\,, \tag{5}$$

$$\frac{d\mathbf{v}_i}{dt} = -\sum_j m_j \left(\frac{P_i}{\rho_i^2} + \frac{P_j}{\rho_j^2} + \Pi_{ij}\right) \nabla_i W_{ij} + \mathbf{f}_i\,, \tag{6}$$

$$\frac{de_i}{dt} = \frac{1}{2}\sum_j m_j \left(\frac{P_i}{\rho_i^2} + \frac{P_j}{\rho_j^2} + \Pi_{ij}\right) \mathbf{v}_{ij} \cdot \nabla_i W_{ij}\,, \tag{7}$$

where $\mathbf{q}_i$ is the particle vector position $[x_i, y_i]^T$, $\mathbf{q}_{ij} = \mathbf{q}_i - \mathbf{q}_j$, $W_{ij} = W(\mathbf{q}_{ij})$, $\mathbf{v}_{ij} = \mathbf{v}_i - \mathbf{v}_j$, $\mathbf{f}_i$ is the sum of external forces normalized by the mass m_i, and Π_{ij} is a dissipative term called *artificial viscosity* added to handle shocks.

There are several variants for the viscosity term, the most common of which is given by [10]:

$$\Pi_{ij} = \begin{cases} \frac{1}{\overline{\rho}_{ij}}(-\xi_1 \overline{c}_{ij}\mu_{ij} + \xi_2 \mu_{ij}^2) & \text{if} \quad \mathbf{v}_{ij} \cdot \mathbf{q}_{ij} < 0\,, \\ 0 & \text{if} \quad \mathbf{v}_{ij} \cdot \mathbf{q}_{ij} > 0\,, \end{cases} \tag{8}$$

where

$$\mu_{ij} = \frac{h\mathbf{v}_{ij} \cdot \mathbf{q}_{ij}}{\|\mathbf{q}_{ij}\|^2 + \eta^2}. \tag{9}$$

In (8), $\overline{\rho}_{ij}$ is the average between the densities of i and j, ξ_1 and ξ_2 are positive viscosity constants, $\overline{c}_{ij}$ is the average speed of sound, and η^2 is a term added to avoid singularities.

The motion of *incompressible fluids* can also be simulated using the SPH method. The key idea is to make a compressible fluid behave like a nearly incompressible one. This can be done by using the equation of state [11]:

$$P_i = B_i \left[\left(\frac{\rho_i}{\rho_0}\right)^{\gamma} - 1\right], \tag{10}$$

where ρ_0 is the reference density ($1000kg/m^3$ in the case of water), γ is the ratio of specific heats, and B_i is the bulk modulus. The bulk modulus is computed to guarantee a small Mach number, M, (typically $0.1 - 0.01$). The following expression may be used [11]:

$$B_i = \left(\frac{\|\mathbf{v}\|_{max}}{M}\right)^2 \rho_i\,, \tag{11}$$

where $\|\mathbf{v}\|_{max}$ is the maximum velocity of the flow. For liquids, the speed of sound of a particle i, which represents the speed at which sound travels through the fluid element represented by the particle, is given by $c_i = \sqrt{B_i/\rho_i}$.

The authors of [12] proposed decentralized controllers for large groups of robots based on the SPH method. In [12], the SPH equations for compressible fluids were used to mimick the behavior of air at 20^o C. In our previous work [13] the SPH method was used to provide decentralized controllers in a *pattern generation task* with static obstacles. In the next section, we present extensions of the technique in [13].

III. CONTROL POLICY

We assume that each robot of the team is a SPH particle subjected to an external force, and since we use kernels with compact support, it is possible to derive decentralized control laws based on the SPH equations. The resulting controllers are decentralized in the sense that only local information is necessary: the gradient of a potential function at the location of the robot i and position and velocity of the robot i itself and of the robots in the neighborhood of i. For a robot i with configuration $\mathbf{q}_i = [x_i, y_i]^T$ we define $\mathcal{N}_i$ as the set of robots in the neighborhood of robot i:

$$\mathcal{N}_i = \{j \neq i \mid \|\mathbf{q}_j - \mathbf{q}_i\| < D\}. \tag{12}$$

The distance D is determined by the kernel support size, which in the case of the kernel in (4) is given by $D = 2h$.

A. Global Potential Functions

Our approach relies on the computation of a global potential function. In this subsection we present two examples of such functions: *harmonic functions* [13] and *shape functions* [9]. Harmonic functions can be efficiently computed in obstacle-filled environments. To numerically compute these functions, we use the Finite Element Method (FEM). The efficiency of such a method is due to its ability to work properly with unstructured meshes which are used to exactly decompose the solution domain.

If a safety factor, ϵ, is defined such that the desired pattern is represented by a region between two curves Γ_1 and Γ_2, we can define a harmonic function which drives the robots toward the goal region and at the same time drives the robots away from the obstacles. If the desired pattern, Γ, is parameterized by a function $s(x, y) = 0$, then Γ_1 is such that $s(x, y) = \epsilon$ and Γ_2 is such that $s(x, y) = -\epsilon$.

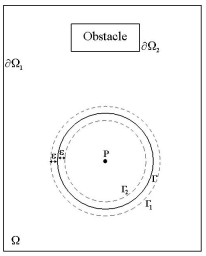

Fig. 2. Domain example.

Figure 2 presents an example of a domain with a circular pattern. Harmonic functions are solutions to the Laplace's equation. In order to guarantee uniqueness in the solution, we must define boundary conditions. We use constant Dirichlet boundary conditions such that a maximum value is obtained at the boundaries of the configuration space and a minimum value is obtained at the desired pattern. This boundary value problem (BVP) is given by:

$$\begin{cases} \nabla^2\phi = 0\,, \\ \Gamma_1 = \Gamma_2 = 0\,, \\ \partial\Omega_1 = \partial\Omega_2 = P = V_c\,, \end{cases} \tag{13}$$

where ϕ is the harmonic function, V_c is a positive constant, and P is a point inside desired closed curves (see Fig. 2).

In obstacle-free environments with desired smooth star shapes, we can use shape functions. For a desired curve parameterized by a function $s(x, y) = 0$, a shape function, ϕ, is defined such that ϕ is a positive semi-definite function with a minimum value equal to zero at the boundary Γ. In this case, the pattern may be described in polar coordinates by $r = \varrho(\alpha)$ and the following shape function may be applied:

$$\phi = \left((r - \varrho(\alpha)) \circ f\right)^2, \tag{14}$$

where $f : (x, y) \to (\alpha, r)$.

B. Holonomic Point Robot Abstraction

Our controller is derived by considering each robot as a SPH particle at $\mathbf{q}_i = [x_i, y_i]^T$ subjected to an external force given by the descent gradient of a global potential function. Under the assumption of fully-actuated, holonomic, point robots, each robot's acceleration is given by $\ddot{\mathbf{q}}_i = \mathbf{u}_i(\mathbf{q}, t)$, where $\mathbf{q} = [\mathbf{q}_1^T, \ldots, \mathbf{q}_N^T]^T$. The controller for each robot is:

$$\mathbf{u}_i(\mathbf{q}) = \mathbf{b}_i - \zeta\mathbf{v}_i + k\mathbf{f}_i\,, \tag{15}$$

where

$$\mathbf{b}_i = -\sum_j m_j \left(\frac{P_i}{\rho_i^2} + \frac{P_j}{\rho_j^2} + \Pi_{ij}\right)\nabla_i W_{ij}\,, \tag{16}$$

k and ζ are positive constants and $\mathbf{f}_i$ is given by a vector defined by $-\nabla\phi$. In fact, we use vector fields of the form:

$$\mathbf{f}_i = \begin{cases} -\frac{\nabla\phi(\mathbf{q}_i)}{\|\nabla\phi(\mathbf{q}_i)\|^\beta} & \text{if } \nabla\phi(\mathbf{q}_i) \neq 0 \\ 0 & \text{if } \nabla\phi(\mathbf{q}_i) = 0 \end{cases}, \tag{17}$$

where β is a non-negative integer number. In (15) we include a dissipative term proportional to $\mathbf{v}_i$, which represents a damping to stabilize the system. It is important to mention that $\mathbf{u}_i(\mathbf{q})$ in (15) can be computed by taking into account only robots in the neighborhood $\mathcal{N}_i$ defined in (12) due to the compact support of the kernel, W. Figure 3 presents a simulation with 121 point robots with control law given by (15). Additional simulations can be found in [13].

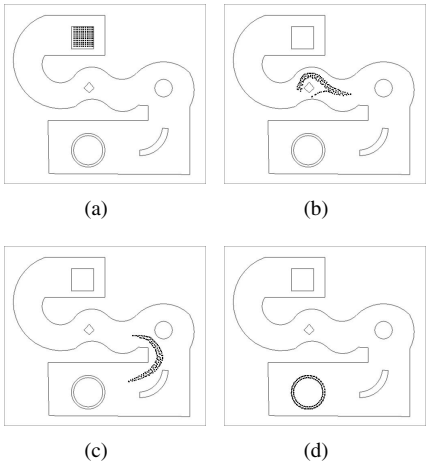

Fig. 3. Simulation with 121 point robots from a starting configuration (Fig. 3(a)) to the goal (Fig. 3(d)), with intermediate configurations (Figs. 3(b) and 3(c)).

C. Finite-size, Nonholonomic Robots

Now, we will describe how our approach may be adapted to take into account actual robot issues. The first issue we address is the finite size of actual robots. The static obstacles are directly taken into account since we plan our potential functions in the robots configuration space. We also assume that our robots are circular in shape with radius R. Given two robots, we guarantee that the robots do not collide with each other if $\|\mathbf{q}_{ij}\| \geq 2R + \varepsilon$, where ε is a safety factor. The collision avoidance of our approach is performed by the artificial viscosity term in (8) with

$$\mu_{ij} = \frac{h\mathbf{v}_{ij} \cdot \mathbf{q}_{ij}}{(\|\mathbf{q}_{ij}\| - (2R + \varepsilon))^2}. \tag{18}$$

This adaptation guarantees a repulsive term in (16) between robots which are moving toward each other. This term is repulsive since $\Pi_{ij} \geq 0$ and $\nabla_i W_{ij}$ points in the direction of $-\mathbf{q}_{ij}$. Note that $\Pi_{ij} \to \infty$ when $\|\mathbf{q}_{ij}\| \to (2R + \varepsilon)$, *i.e.*, when the robots are about to collide.

Besides the robot size, motion constraints are also an important consideration. In our experiments we use differential drive, kinematically controlled robots. To control such robots we use feedback linearization:

$$\begin{bmatrix} v \\ \omega \end{bmatrix} = \begin{bmatrix} \cos(\theta) & \sin(\theta) \\ -\frac{\sin(\theta)}{d} & \frac{\cos(\theta)}{d} \end{bmatrix} \cdot \begin{bmatrix} \dot{x}_d \\ \dot{y}_d \end{bmatrix}, \tag{19}$$

where v and ω are linear and angular velocities, respectively, and θ is the robot orientation. The parameter d defines a point, $[x_d, y_d]^T$, in the global frame, which corresponds to $[d, 0]^T$ in the robot frame. Now, each robot is represented in its configuration space by the point $[x_{d_i}, y_{d_i}]^T$ such that the physical extent of the robot lies within the circle of center

$[x_{d_i}, y_{d_i}]^T$ and radius $R' = R + d$. The SPH particles are also placed at the points $[x_{d_i}, y_{d_i}]^T$. Since our controllers were devised for robots fully actuated in their acceleration we compute the integral $[\dot{x}_{d_i}, \dot{y}_{d_i}]^T = \int \mathbf{u}_i(\mathbf{q})dt$.

D. Virtual Particles

When controlling multiple robots, due to the presence of inter-particle forces, $\mathbf{b}_i$, the external force, $\mathbf{f}_i$, may be not enough to avoid collisions. We add virtual particles right at the boundaries of the configuration space such that we can guarantee collision avoidance. In fact, we want to take advantage of the collision avoidance property provided by the artificial viscosity. There are several ways of implementing this virtual particle idea. One option is to create a virtual particle at the closest boundary point, $\mathbf{p}$. Then we adapt the term $\mathbf{b}_i$ in (16) such that:

$$\begin{aligned}\mathbf{b'}_i = &-\sum_j m_j \left(\frac{P_i}{\rho_i^2} + \frac{P_j}{\rho_j^2} + \Pi_{ij}\right)\nabla_i W_{ij}(h) \\ &- \lambda \Pi_{ip} \nabla_i W_{ip}(h')\,,\end{aligned} \tag{20}$$

where λ is a positive constant, j iterates only through the N particles that represent real robots, and p refers to the virtual particle. Due to the fact that the size of the robot is already taken into account in the configuration space, we use $R = 0$ in (18). Note that the virtual particle does not change the density ρ_i and also does not have its own density. The other terms necessary to compute Π_{ip} are $\overline{\rho}_{ip} = \rho_i$ and $\overline{c}_{ip} = c_i$.

Another option is to assign virtual particles to each cell with obstacle in a local occupancy grid. This option was found to be the most robust during experiments.

IV. ANALYSIS

Our stability and convergence analysis is built upon the results in [9]. The next four results correspond to our version of the Results 4.1 to 4.4 in [9]. We assume obstacle-free environments and $\mathbf{f}_i$ in (15) is given by $-\nabla\phi$, where ϕ is the shape function in (14). We also assume that the robots are represented by identical SPH particles with mass m.

Before presenting our results we define the function $\phi_S(\mathbf{q})$ as a measure of performance that should be minimized:

$$\phi_S(\mathbf{q}) = k \sum_i \phi(\mathbf{q}_i). \tag{21}$$

Proposition 1 *Given a system of N point robots with dynamics $\ddot{\mathbf{q}}_i = \mathbf{u}_i(\mathbf{q}, t)$ and a control law determined by (15), where $\mathbf{f}_i = -\nabla\phi$ and ϕ is a shape function, the system equilibrium points are at an extremum of ϕ_S.*

Proof: Since the system is in equilibrium we have $\ddot{\mathbf{q}} = 0$ and $\dot{\mathbf{q}} = 0$. We have also $\Pi_{ij} = 0$ and $\mathbf{u}_i = 0$. Therefore, $\sum_i \mathbf{u}_i = 0$. Since $\nabla_i W_{ij} = -\nabla_j W_{ij}$, we have $\sum_i \mathbf{u}_i = k\sum_i \nabla\phi_i = 0$. However, $k\sum_i \nabla\phi_i = 0$ is the necessary condition for ϕ_S to be at an extremum. ■

Proposition 2 *Consider the positive semi-definite function:*

$$V = \phi_S + \sum_i (e'_i - e_0) + \frac{1}{2}\mathbf{v^T v}\,, \tag{22}$$

where e'_i is the part of the internal energy related to conservative forces such that:

$$\frac{de'_i}{dt} = \frac{1}{2}\sum_j m \left(\frac{P_i}{\rho_i^2} + \frac{P_j}{\rho_j^2}\right)\mathbf{v}_{ij}\cdot\nabla_i W_{ij} \tag{23}$$

and e_0 is the minimum internal energy which is obtained when $\mathbf{v}_i = 0$ and $\rho_i = \rho_0$ for all i. Consider also the set $\Omega_c = \{\mathbf{x} \in X | V(\mathbf{q}, \mathbf{v}) \leq c\}$, where X is the state space defined by $\mathbf{x} = [\mathbf{q}_1^T \mathbf{v}_1^T \ldots \mathbf{q}_N^T \mathbf{v}_N^T]^T$. Given the set S with boundary determined by the desired pattern Γ and the system of robots defined in Proposition 1 with initial conditions $\mathbf{x}_0 \in \Omega_c$, the system converges to an invariant set, $\Omega_I \subset \Omega_c$, such that the points in Ω_I minimize the measure function ϕ_S.

Proof: Since V is continuous, we conclude that Ω_c is closed for some $c > 0$. Also, due to the fact that $\phi_S + \sum_i (e'_i - e_0) \leq c$ and $\mathbf{v}^T\mathbf{v} \leq c$ we conclude that Ω_c is compact.

We have that

$$\dot{V} = \sum_i (k\nabla\phi_i^T \dot{\mathbf{q}}_i + \mathbf{v}_i^T \dot{\mathbf{v}}_i) + \sum_i \frac{de'_i}{dt}. \tag{24}$$

By using (15) and (23), and the fact that $\nabla_i W_{ij} = -\nabla_j W_{ji}$ and $\Pi_{ij} = \Pi_{ji}$

$$\dot{V} = -\sum_i \zeta \mathbf{v}_i^T \mathbf{v}_i - \sum_i \frac{1}{2}\sum_j m\Pi_{ij}\mathbf{v}_{ij}^T \nabla_i W_{ij} \leq 0.$$

By using the LaSalle's Invariance Principle, we conclude that for any $\mathbf{x}_0 \in \Omega_c$ the system converges asymptotically to the largest invariant set $\Omega_I = \{\mathbf{x} \in X | \dot{V} = 0\}$, which corresponds to $\mathbf{v}_i = 0\ \forall i$ with $\Omega_I \subset \Omega_c$. Since Ω_I contains all equilibrium points in Ω_c and based on the Proposition 1 we conclude that all points in Ω_I minimize ϕ_S. ■

Proposition 3 *Consider the set Ω_S defined by*

$$\Omega_S = \{\mathbf{x} | \phi(\mathbf{q}_i) = 0, \mathbf{v}_i = 0, \rho_i = \rho_0 \forall i\}\,, \tag{25}$$

where ϕ is a shape function. Given the system of N robots defined in Proposition 1, the set Ω_S is a stable submanifold and $\Omega_S \subset \Omega_I$.

Proof: Since $\mathbf{v}_i = 0$ for all i, $\Omega_S \subset \Omega_I$. The potential energy of the system is given by $U = \phi_S + \sum_i e'_i$. We need to show that the hessian of U, $\mathbf{H}_U = \mathbf{H}_{\phi_S} + \mathbf{H}_{\sum_i e'_i}$, is positive semi-definite when $\mathbf{q}_i \in \Gamma$ and $\rho_i = \rho_0\ \forall i$.

It is proved in [9] that the $2N \times 2N$ matrix $\mathbf{H}_{\phi_S}$ is positive semi-definite when $\phi(\mathbf{q}_i) = 0$. Therefore, we need to prove that $\mathbf{H}_{\sum_i e'_i} \geq 0$ when $\rho_i = \rho_0$. By using $\nabla_i W_{ij} = -\nabla_j W_{ji}$ in (23) we can write after some algebra

$$\frac{\partial \sum_n e'_n}{\partial \mathbf{q}_i} = \sum_j m \left(\frac{P_i}{\rho_i^2} + \frac{P_j}{\rho_j^2}\right)\nabla_i W_{ij}. \tag{26}$$

After using the state equation (10), computing the second derivatives, and using $\rho_i = \rho_0$, we can obtain

$$\mathbf{H}_{\sum_i e'_i} = \frac{m^2\gamma\sigma}{\rho_0^2}\mathbf{A}\mathbf{A}^T \geq 0\,, \tag{27}$$

where σ is a positive constant and

$$\mathbf{A} = \begin{pmatrix} \sum_k \partial \frac{W_{1k}}{\partial x_1} & \partial \frac{W_{12}}{\partial x_1} & \dots & \partial \frac{W_{1N}}{\partial x_1} \\ \sum_k \partial \frac{W_{1k}}{\partial y_1} & \partial \frac{W_{12}}{\partial y_1} & \dots & \partial \frac{W_{1N}}{\partial y_1} \\ \vdots & \vdots & \vdots & \vdots \\ \partial \frac{W_{N1}}{\partial x_N} & \partial \frac{W_{N2}}{\partial x_N} & \dots & \sum_k \partial \frac{W_{Nk}}{\partial x_N} \\ \partial \frac{W_{N1}}{\partial y_N} & \partial \frac{W_{N2}}{\partial y_N} & \dots & \sum_k \partial \frac{W_{Nk}}{\partial y_N} \end{pmatrix}.$$

■

Proposition 4 *For any smooth star shape, Γ, the system of N robots defined in Proposition 1, with $\rho_i = \rho_0$ $\forall i$ during all instants of time t, converges to Γ for any $\mathbf{x}_0 \in \Omega_c$.*

Proof: If $\rho_i = \rho_0$, $\forall i$, during all instants of time t, then the equilibrium of the system is given by $\nabla_i \phi(\mathbf{q}_i) = 0$, $\forall i$. Proposition 2 guarantees the system converges to Ω_I. As proven in [9] we have that $\nabla_i \phi(\mathbf{q}_i) = 0$ if and only if $\mathbf{q}_i \in \Gamma$. Therefore $\Omega_I \equiv \Omega_S \equiv \Gamma$. ■

Next, we present results concerning collision avoidance.

Proposition 5 *Given a pair of robots, i and j, with radius R, dynamics $\ddot{\mathbf{q}}_i = \mathbf{u}_i(\mathbf{q}, t)$, and control law (15), where μ_{ij} is given by (18), the robots will never collide with each other.*

Proof: The worst case happens when the robots i and j drive with opposite maximum finite velocities $\mathbf{v}_m$ and $-\mathbf{v}_m$, respectively, and $\mathbf{b}_i$ and $\mathbf{f}_i$ assume constant maximum finite values in the direction $\mathbf{q}_{ji}$, and $\mathbf{b}_j$ and $\mathbf{f}_j$ assume constant maximum finite values in the direction $\mathbf{q}_{ij}$. Since $-\nabla_i W_{ij}$ points in the direction of $\mathbf{q}_{ij}$ and $\Pi_{ij} \geq 0$ we conclude that the term given by the artificial viscosity is a repulsive term. Due to the symmetry we have in this case $\mathbf{v}_i = -\mathbf{v}_j$. Further, by checking the expression of μ_{ij} in (18) one should notice that the artificial viscosity term corresponds to a nonlinear damping $-F(\mathbf{q}_i, \mathbf{q}_j)v_i - G(\mathbf{q}_i, \mathbf{q}_j)v_i^2$, where $F \geq 0$ and $G \geq 0$. The artificial viscosity is active in the interval $\|\mathbf{q}_{ij}\| < 2h$, and since $F \to +\infty$ and $G \to +\infty$ when $\|\mathbf{q}_{ij}\| \to (2R + \varepsilon)$ we can guarantee that $\mathbf{v}_i \to 0$ somewhere in the interval $2R + \varepsilon \leq \|\mathbf{q}_{ij}\| < 2h$. Due to symmetry we can guarantee that $\mathbf{v}_{ij} \cdot \mathbf{q}_{ij} \geq 0$ when $\|\mathbf{q}_{ij}\| \to 2R + \varepsilon$. ■

Proposition 6 *Given a robot, i, with dynamics $\ddot{\mathbf{q}}_i = \mathbf{u}_i(\mathbf{q}, t)$, and the control law determined by (15), with virtual particles defined as in Subsection III-D, the robot will never collide with static obstacles.*

Proof: We just need to guarantee that $\mathbf{v}_i \cdot (\mathbf{q}_i - \mathbf{p}) \geq 0$ when $\|\mathbf{q}_i - \mathbf{p}\| - \varepsilon \to 0$, where $\mathbf{p}$ is the closest point in the boundary of the configuration space. We have that $\mathbf{v}_p = 0$ and $\mathbf{b'}_i$ is determined by (20). The arguments of the proof of Proposition 5 complete the proof. ■

V. EXPERIMENTAL AND SIMULATION RESULTS

In this section, we present experimental and simulation results that verify the proposed approach for finite size and nonholonomic robots. Movies can be seen on the web page http://kumar.cis.upenn.edu/∼lucpim/icra2008.

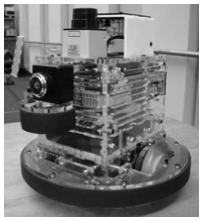

Fig. 4. The 20 × 13.5 × 22.2 cm^3 differential drive robotics platform.

In the experiments we used a team of seven differential drive, kinematically controlled robots called *Scarabs* (see Fig. 4). Details of the Scarabs are described in [14]. The team of robots were provided with a map of the environment which was defined by the boundaries of the experimental area and static obstacles. A vector field based on harmonic functions was computed off-line. Each robot computed its location in the map based on localization information from an overhead tracking system and current velocity from its motor controller. This information was broadcasted over the network to the other robots. To emulate the notion of neighborhoods in the smaller experimental area, each robot ignored messages from robots a distance greater than 2 m. At every update of the control algorithm, each robot computed its current SPH state based on its local information and the information received over the network. Additionally, each robot incorporated virtual particles based on the map within a region $2h' \times 2h'$, with $h' = 0.3$ m.

A vignette of one trial run of the implementation is shown in Fig. 5. The control law was executing at an update rate of 10 Hz while the inter-agent network communications were executing at a higher rate of 20 Hz to accommodate the asynchronous system design. One can see that two robots did not converge to the goal. This was due to limitations of the minimum allowed velocities of the actual robots. Since one of the robots that had already reached the goal was not moving, the two other ones could not converge.

We implemented simulations using the 3D environment GAZEBO [15], which allows for simulating conditions that are very close to the real world ones. We used robot models that capture the geometry, kinematics, and dynamics of the Scarab robots. Moreover, we considered a virtual world with the same dimensions of the area where the experiments were performed. The obstacles and the goal were also the same. A simulation trial with 15 robots is presented in Fig. 6.

VI. CONCLUSIONS

In this work we extended the results of a novel decentralized approach to control swarms of robots presented in [13] to the case of finite size and differential drive robots. We used the SPH technique to model the swarm as an incompressible fluid and also a global potential function that allows for solving the pattern generation task in the presence of obstacles. We chose the potential function to be a harmonic function. The Finite Element Method was used to compute this function which guarantees efficiency in

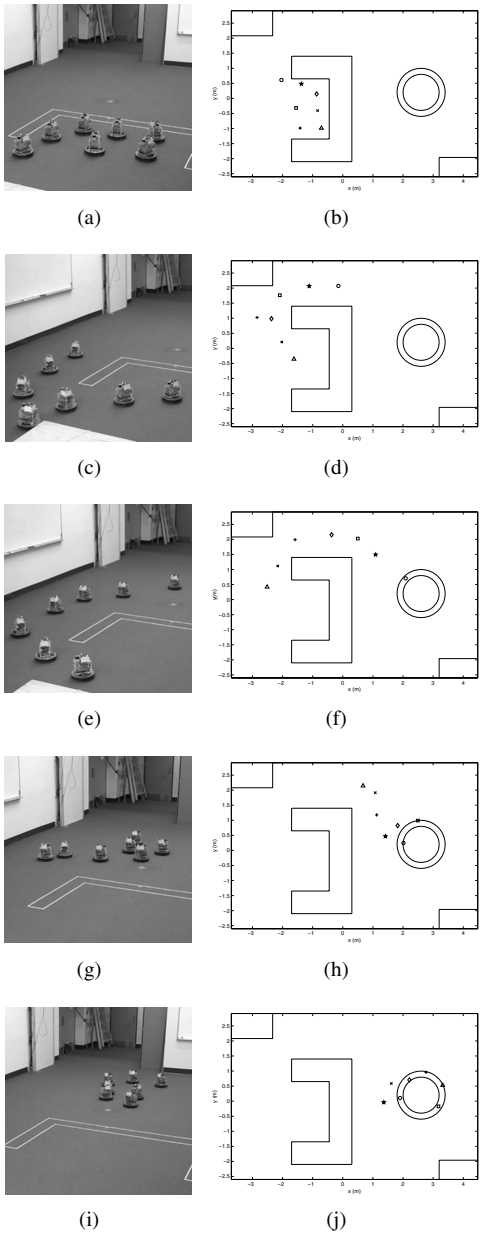

Fig. 5. Experimental Results. A team of seven robots, starting from an initial configuration (Fig. 5(a)), control around an obstacle (Figs. 5(c), 5(e), and 5(g)) to a goal circular formation (Fig. 5(i)). The results in the configuration space are also shown in Figs. 5(b), 5(d), 5(f), 5(h), and 5(j).

geometrically complicate domains. By adapting the artificial viscosity term and also by including virtual particles we were able to guarantee that the robots are driven safely. For obstacle-free environments we used shape functions and proved stability and convergence of our controllers.

Our approach is scalable and there is no need for labelling the robots. The approach is also robust to dynamic deletion and addition of agents. Since the robots try to keep the density of the fluid model constant, this approach allows for a loose way of controlling the group connectivity.

VII. ACKNOWLEDGMENTS

The authors would like to acknowledge the financial support of CNPq – Brazil, ARO MURI SWARMS Grant W911NF-05-1-0219, and the NSF ITR Grant 0324977.

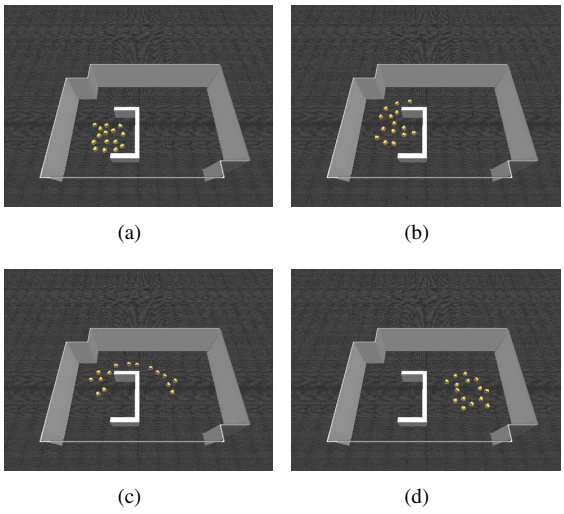

Fig. 6. Simulation with 15 robots from a starting configuration (Fig. 6(a)) to the goal (Fig. 6(d)), with intermediate configurations (Figs. 6(b) and 6(c)).

REFERENCES

[1] M. Shimizu, A. Ishiguro, T. Kawakatsu, Y. Masubuchi, and M. Doi, "Coherent swarming from local interaction by exploiting molecular dynamics and stokesian dynamics methods," in *Proc. IEEE/RSJ Int. Conf. Intel. Robots and Systems*, vol. 2, 2003, pp. 1614 – 1619.

[2] W. Kerr and D. F. Spears, "Robotic simulation of gases for a surveillance task," in *Proc. IEEE/RSJ Int. Conf. Intel. Robots and Systems*, 2005, pp. 2905–2910.

[3] K. Sugihara and I. Suzuki, "Distributed algorithms for formation of geometric patterns with many mobile robots," *Journal of Robotic Systems*, vol. 13, no. 3, pp. 127–139, 1996.

[4] J. P. Desai, J. P. Ostrowski, and V. Kumar, "Modeling and control of formations of nonholonomic mobile robots," *IEEE Trans. Robot. and Automat.*, vol. 17, no. 6, pp. 905–908, 2001.

[5] H. C.-H. Hsu and A. Liu, "Multiple teams for mobile robot formation control," in *Proceedings of the IEEE International Symposium on Intelligent Control*, 2004, pp. 168–173.

[6] T. Balch and R. C. Arkin, "Behavior-based formation control for multirobot teams," *IEEE Trans. Robot. and Automat.*, vol. 14, no. 6, pp. 926–939, 1998.

[7] Z. Cao, M. Tan, S.Wang, Y. Fan, and B. Zhang, "The optimization research of formation control for multiple mobile robots," in *Proc. of the 4th World Congress on Intel. Control and Automat.*, 2002, pp. 1270–1274.

[8] L. Chaimowicz, N. Michael, and V. Kumar, "Controlling swarms of robots using interpolated implicit functions," in *Proc. IEEE Int. Conf. Robot. Automat.*, Barcelona, Spain, April 2005, pp. 2498–2503.

[9] M. A. Hsieh and V. Kumar, "Pattern generation with multiple robots," in *Proc. IEEE Int. Conf. Robot. Automat.*, Orlando, USA, May 2006, pp. 2442–2447.

[10] J. J. Monaghan, "Smoothed particle hydrodynamics," *Annual Review of Astronomy and Astrophysics*, vol. 30, pp. 543–574, 1992.

[11] ——, "Simulating free surface flow with SPH," *Journal of Computational Physics*, vol. 110, pp. 399–406, 1994.

[12] J. R. Perkinson and B. Shafai, "A decentralized control algorithm for scalable robotic swarms based on mesh-free particle hydrodynamics," in *Proc. of the IASTED Int. Conf. on Robot. and Applications*, 2005, pp. 1–6.

[13] L. C. A. Pimenta, M. L. Mendes, R. C. Mesquita, and G. A. S. Pereira, "Fluids in electrostatic fields: An analogy for multi-robot control," *IEEE Trans. on Magnetics*, vol. 43, no. 4, pp. 1765 – 1768, 2007.

[14] N. Michael, J. Fink, and V. Kumar, "Experimental testbed for large multi-robot teams: Verification and validation," *IEEE Robotics and Automation Magazine*, Mar. 2008, to Appear.

[15] B. Gerkey, R. T. Vaughan, and A. Howard, "The Player/Stage project: Tools for multi-robot and distributed sensor systems," in *Proc. of the Int. Conf. on Advanced Robotics*, 2003, pp. 317–323.